HAL open science

The large-scale magnetic field and poleward mass accretion of the classical T Tauri star TW Hya

J. -F. Donati, S. G. Gregory, S. H. P. Alencar, J. Bouvier, G. Hussain, M. Skelly, C. Dougados, M. M. Jardine, F. Ménard, M. M. Romanova, et al.

To cite this version:

J. -F. Donati, S. G. Gregory, S. H. P. Alencar, J. Bouvier, G. Hussain, et al.. The large-scale magnetic field and poleward mass accretion of the classical T Tauri star TW Hya. Monthly Notices of the Royal Astronomical Society, 2011, 417, pp.472-487. 10.1111/j.1365-2966.2011.19288.x . insu-03612372

HAL Id: insu-03612372

https://insu.hal.science/insu-03612372v1

Submitted on 17 Mar 2022

HAL is a multi-disciplinary open access archive for the deposit and dissemination of scientific research documents, whether they are published or not. The documents may come from teaching and research institutions in France or abroad, or from public or private research centers.

L'archive ouverte pluridisciplinaire **HAL**, est destinée au dépôt et à la diffusion de documents scientifiques de niveau recherche, publiés ou non, émanant des établissements d'enseignement et de recherche français ou étrangers, des laboratoires publics ou privés.

Distributed under a Creative Commons Attribution 4.0 International License

Monthly Notices of the ROYAL ASTRONOMICAL SOCIETY

Mon. Not. R. Astron. Soc. **417,** 472–487 (2011) doi:10.1111/j.1365-2966.2011.19288.x

The large-scale magnetic field and poleward mass accretion of the classical T Tauri star TW Hya

J.-F. Donati,[1★] S. G. Gregory,[2] S. H. P. Alencar,[3] J. Bouvier,[4] G. Hussain,[5] M. Skelly,[1] C. Dougados,[4] M. M. Jardine,[6] F. Ménard,[4] M. M. Romanova,[7] Y. C. Unruh[8] and the MaPP collaboration

[1]*IRAP–UMR 5277, CNRS & Univ. de Toulouse, 14 Av. E. Belin, F–31400 Toulouse, France*
[2]*California Institute of Technology, MC 249-17, Pasadena, CA 91125, USA*
[3]*Departamento de Fìsica – ICEx – UFMG, Av. Antônio Carlos, 6627, 30270-901 Belo Horizonte, MG, Brazil*
[4]*IPAG–UMR 5274, CNRS & Univ. J. Fourier, 414 rue de la Piscine, F–38041 Grenoble, France*
[5]*ESO, Karl-Schwarzschild-Str. 2, D-85748 Garching, Germany*
[6]*School of Physics and Astronomy, University of St Andrews, St Andrews KY16 9SS*
[7]*Department of Astronomy, Cornell University, Ithaca, NY 14853-6801, USA*
[8]*Astrophysics Group, Blackett Laboratory, Imperial College London, London SW7 2AZ*

Accepted 2011 June 20. Received 2011 June 20; in original form 2011 May 25

ABSTRACT

We report here results of spectropolarimetric observations of the ≃8 Myr classical T Tauri star (cTTS) TW Hya carried out with ESPaDOnS at the Canada–France–Hawaii Telescope in the framework of the 'Magnetic Protostars and Planets' programme, and obtained at two different epochs (2008 March and 2010 March). Obvious Zeeman signatures are detected at all times, both in photospheric lines and in accretion-powered emission lines. Significant intrinsic variability and moderate rotational modulation are observed in both photospheric and accretion proxies.

Using tomographic imaging, we reconstruct maps of the large-scale field of the photospheric brightness and the accretion-powered emission at the surface of TW Hya at both epochs. We find that the magnetic topology is mostly poloidal and axisymmetric with respect to the rotation axis of the star and that the octupolar component of the large-scale field (2.5–2.8 kG at the pole) largely dominates the dipolar component. This large-scale field topology is characteristic of partly convective stars, supporting the conclusion (from evolutionary models) that TW Hya already hosts a radiative core. We also show that TW Hya features a high-latitude photospheric cool spot overlapping with the main magnetic pole (and producing the observed radial velocity fluctuations); this is also where accretion concentrates most of the time, although accretion at lower latitudes is found to occur episodically.

We propose that the relatively rapid rotation of TW Hya (with respect to AA Tau-like cTTSs) directly reflects the weakness of the large-scale dipole, no longer capable of magnetically disrupting the accretion disc up to the corotation radius (at which the Keplerian period equals the stellar rotation period). We therefore conclude that TW Hya is in a phase of rapid spin-up as its large-scale dipole field progressively vanishes.

Key words: techniques: polarimetric – stars: formation – stars: imaging – stars: individual: TW Hya – stars: magnetic field – stars: rotation.

1 INTRODUCTION

Magnetic fields play a significant role throughout the life of stars, all the way from the cradle to the grave (e.g. Donati & Landstreet 2009, for a review). The impact of magnetic fields is strongest during the very first stages of their life, when protostars and their surrounding planetary systems form out of the collapse of giant molecular clouds; in particular, fields are presumably efficient at slowing down the cloud collapse, at inhibiting the subsequent fragmentation and at dissipating the cloud angular momentum through magnetic braking and the magnetized outflows and collimated jets generated as part

★E-mail: donati@ast.obs-mip.fr

© 2011 The Authors
Monthly Notices of the Royal Astronomical Society © 2011 RAS

Downloaded from https://academic.oup.com/mnras/article/417/1/472/980080 by guest on 17 March 2022

of the formation process (e.g. André, Basu & Inutsuka 2009). In the latter phases, when low-mass protostars are still actively collecting mass from their surrounding accretion disc, the large-scale magnetic fields that the protostars generate (through dynamo processes) are strong enough to disrupt the inner disc regions, funnel the disc material to the stellar surface and drastically brake the rotation of the protostar (see e.g. Bouvier et al. 2007a, for a review).

Magnetic fields at the surfaces of classical T Tauri stars (cTTSs) were first reported indirectly through the detection of various spectral proxies, usually continuum or line emission throughout the whole electromagnetic spectrum, from X-rays to radio wavelengths. It is only about two decades ago that fields of cTTSs were first detected directly, i.e. through the Zeeman broadening of spectral lines, and found to reach typical magnetic intensities of several kG (e.g. Johns-Krull 2007, for an overview). However, the actual large-scale topologies of these fields, controlling in particular how the fields couple the protostars to their discs, redirect the accreted disc material and subsequently brake the stellar rotation, remained unclear until recently. Thanks to the advent of sensitive high-resolution spectropolarimeters dedicated to the study of stellar magnetic fields, it is now possible to monitor polarized Zeeman signatures of cTTSs in various spectral lines (e.g. those probing accreting and non-accreting regions at the stellar surface) and use such time series to reconstruct the parent large-scale magnetic topologies of cTTSs (following the principles of tomographic imaging); this option offers in particular a more quantitative way of studying magnetospheric accretion processes of cTTSs.

This is precisely the main goal of the international Magnetic Protostars and Planets (MaPP) project, designed to investigate (through a first survey of a dozen targets) how the large-scale magnetic topologies of cTTSs vary with stellar parameters such as mass, age, rotation and accretion rates (e.g. Donati et al. 2010, ,2011a). MaPP also aims at providing an improved theoretical description of the observational results, using both analytical modelling and numerical simulations (see e.g. Gregory et al. 2010; Romanova et al. 2011) – the ultimate ambition being to obtain a deeper understanding of magnetic field generation and magnetospheric accretion processes in cTTSs and of their impact on the formation of low-mass stars. Results up to now demonstrate in particular that the large-scale magnetic fields of cTTSs closely resemble those of low-mass main-sequence dwarfs (once both samples are matched according to their internal structure), with high-mass fully convective cTTSs (with masses ranging from about 0.5 to 1.0 $M_\odot$ typically, for ages of a few Myr) hosting strong axisymmetric dipoles, while partly convective cTTSs (of either higher masses and/or ages) exhibit a more complex field and a much weaker (potentially non-axisymmetric) dipole component.

The new study presented in this paper focuses on the evolved cTTS TW Hya, whose relative proximity to the Earth and intense magnetic fields (Yang, Johns-Krull & Valenti 2005, 2007) make it an obvious target of investigation for MaPP. With an age of about 8 Myr (e.g. Torres et al. 2008) and a mass of about 0.8 $M_\odot$ (see Section 2), TW Hya can be viewed as an evolved version of two other prototypical cTTSs, namely AA Tau and BP Tau, and can thus serve as a landmark to test new generation models of stellar formation including the effect of magnetic fields. After summarizing the main characteristics of TW Hya (Section 2), we describe the new spectropolarimetric observations we collected (Section 3) and outline the associated temporal variability and rotational modulation (Section 4). We then detail the modelling of these data with our magnetic imaging code (Section 5), briefly compare our results with those published already and conclude with a updated summary of what MaPP results tell us about how magnetic fields impact the formation of Sun-like stars (Section 6).

2 TW HYA

TW Hya (K6V) is one of the low-mass cTTSs located nearest to the Earth (at a distance of 57 ± 7 pc); it belongs to a loose association of young stars after which it was named (the TW Hya association), whose age is estimated to be ≃8 Myr, i.e. somewhat younger than the β Pic moving group, another nearby young association (e.g. Torres et al. 2008).

Despite being older than most prototypical cTTSs, TW Hya is still surrounded by a relatively massive accretion disc visible at infrared (IR) and radio wavelengths, and subject to intense scrutiny in the last decade (e.g. Qi et al. 2004; Thi et al. 2010). With a typical mass of a few Jupiter masses, this disc is found to be inclined at ≃10° to the plane of the sky; it consists at least of an optically thin inner cavity extending outwards up to about 4 au and of an optically thick outer disc extending to distances of up to about 200 au (e.g. Calvet et al. 2002; Akeson et al. 2011), suggesting that planet formation is ongoing. The gas-to-dust mass ratio in the disc may be lower than the standard interstellar value, suggesting that a significant fraction of the primordial disc gas has been evaporated due to the strong X-ray flux from the central protostar (Thi et al. 2010).

The photospheric temperature of TW Hya estimated from the strength of spectral lines is found to be around 4150 K (Torres et al. 2003; Yang et al. 2005), only slightly hotter than the value of 4000 K that the $V - R$ and $V - I$ photometric colours indicate (Rucinski & Krautter 1983; Rucinski et al. 2008); we therefore choose a temperature of 4075 ± 75 K as a compromise. From this temperature, evolutionary models (e.g. Siess, Dufour & Forestini 2000) indicate that the parent protostar (whose contraction is still mostly isothermal at an age of 8–10 Myr) has a typical mass of 0.8 $M_\odot$, a logarithmic luminosity (with respect to the Sun) of –0.45 and radius of 1.1 $R_\odot$. This agrees well with the brightest photometric level recorded for TW Hya ($m_V = 10.6$; e.g. Rucinski et al. 2008), the distance modulus derived from the *Hipparcos* distance (3.75 ± 0.25) and the bolometric correction corresponding to the photospheric temperature (−0.95 ± 0.05; e.g. Bessell, Castelli & Plez 1998), yielding a bolometric magnitude of 5.90 ± 0.25, i.e. a logarithmic luminosity (with respect to the Sun) of −0.46 ± 0.10 (see Fig. 1). Evolutionary models also indicate that, at this age, TW Hya is likely no longer fully convective and hosts a radiative core extending up to ≃0.35 $R_\star$ in radius (Siess et al. 2000).

The spectrum of TW Hya was recently found to undergo regular radial velocity (RV) fluctuations with a period of 3.56 d, first attributed to a close-in giant planet (Setiawan et al. 2008), then to the presence of dark spots at the surface of the star (better reproducing in particular how the RV amplitude varies with wavelength; Huélamo et al. 2008). It therefore strongly suggests that the period of the RV fluctuations is the rotation period of TW Hya, implying an equatorial rotation velocity of 15.6 km s^{-1} (given the assumed radius of 1.1 $R_\odot$; see above). Numerous estimates of the line-of-sight projected equatorial rotation velocity (noted $v \sin i$, where i is the inclination of the rotation axis to the line of sight) are available in the literature, ranging from 4 to 15 km s^{-1} (Torres et al. 2003); the most reliable of these estimates (those including a basic modelling of the micro- and/or macro-turbulent broadening of the spectral lines in particular) are all on the low side of this range (between 4 and 6 km s^{-1}; e.g. Alencar & Batalha 2002; Torres et al. 2003; Yang et al. 2005), consistent with the fact that TW Hya is seen mostly pole-on (as the disc itself). Our own estimate (4 ± 1 km s^{-1}; see

Downloaded from https://academic.oup.com/mnras/article/417/1/472/980080 by guest on 17 March 2022

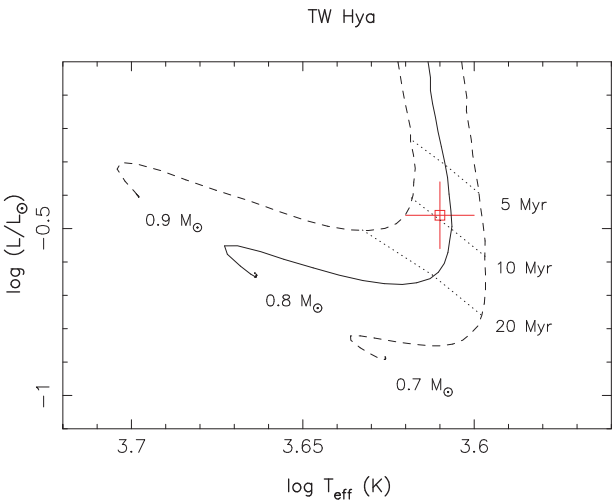

Figure 1. Observed (open square and error bars) location of TW Hya in the HR diagram. The pre-main-sequence evolutionary tracks and corresponding isochrones (Siess et al. 2000) assume solar metallicity and include convective overshooting.

Section 5) implies $i \simeq 15^\circ$, in agreement with previous estimates and with the inclination of the disc (e.g. Alencar & Batalha 2002).

From both magnetic broadening of spectral lines and Zeeman signatures of emission lines used as accretion proxies, kG magnetic fields were recently reported at the surface of TW Hya (Yang et al. 2005, 2007), making it an obvious target for studies of magnetospheric accretion processes. High-resolution X-ray spectra of TW Hya exhibit numerous spectral lines formed at low and high temperatures and allowing one to probe both the accretion shock and the corona (e.g. Kastner et al. 2002; Brickhouse et al. 2010); the low-temperature component of the X-ray spectrum (related to the accretion process) is particularly prominent on TW Hya (with respect to other cTTSs), making it an obvious laboratory for studying the physics of magnetospheric accretion processes. Observations are found to agree reasonably well with the predictions of theoretical models (e.g. Günther et al. 2007).

From the equivalent widths and the corresponding line fluxes of the optical emission lines (taken as accretion proxies) and using the published empirical correlations between lines and accretion fluxes (Fang et al. 2009), we can derive an estimate of the logarithmic mass accretion rate (in units of $\mathrm{M_\odot\,yr^{-1}}$) at the surface of TW Hya, which we find to be equal to -8.9 ± 0.4 at both epochs (see Section 4), in agreement with independent estimates from optical proxies (Curran et al. 2011). As usual, this is larger than the estimate derived from X-ray data (equal to -9.74 ± 0.05; Curran et al. 2011).

Optical veiling, i.e. the apparent weakening of the photospheric spectrum (presumably caused by accretion), is significant in TW Hya and typically ranges from 30 to 100 per cent during both observing runs, in agreement with previous published reports (e.g. Yang et al. 2005).

3 OBSERVATIONS

Spectropolarimetric observations of TW Hya were collected at two different epochs, first from 2008 March 15 to 28, then from 2010 February 23 to March 08, using the high-resolution spectropolarimeter ESPaDOnS on the Canada–France–Hawaii Telescope (CFHT). ESPaDOnS collects stellar spectra spanning the entire optical domain (from 370 to 1000 nm) at a resolving power of 65 000 (i.e. 4.6 km s^{-1}) and with a spectral sampling of 2.6 km s^{-1}, in either circular or linear polarization (Donati 2003). In 2008, a total of 13 circular polarization spectra were collected over a timespan of 14 nights, but with fairly irregular time sampling; in 2010, another set of 13 circular polarization spectra were collected, again over 14 nights, but this time with at a much more regular rate (of about 1 spectrum per night). All polarization spectra (except the first three in 2008 March, affected by a set-up problem) consist of four individual subexposures (each lasting 815 and 840 s in 2008 and 2010, respectively) taken in different polarimeter configurations to allow the removal of all spurious polarization signatures at first order.

All raw frames are processed with Libre ESpRIT, a fully automatic reduction package/pipeline available at CFHT. It automatically performs optimal extraction of ESPaDOnS unpolarized (Stokes I) and circularly polarized (Stokes V) spectra grossly following the procedure described in Donati et al. (1997). The velocity step corresponding to CCD pixels is about 2.6 km s^{-1}; however, thanks to the fact that the spectrograph slit is tilted with respect to the CCD lines, spectra corresponding to different CCD columns across each order feature a different pixel sampling. Libre ESpRIT uses this opportunity to carry out optimal extraction of each spectrum on a sampling grid denser than the original CCD sampling, with a spectral velocity step set to about 0.7 CCD pixel (i.e. 1.8 km s^{-1}). All spectra are automatically corrected of spectral shifts resulting from instrumental effects (e.g. mechanical flexures, temperature or pressure variations) using telluric lines as a reference. Though not perfect, this procedure provides spectra with a relative RV precision of better than 0.030 km s^{-1} (e.g. Donati et al. 2008a).

The peak signal-to-noise ratios (S/N; per 2.6 km s^{-1} velocity bin) achieved on the collected spectra range between 100 and 260 depending on weather/seeing conditions (and on the instrumental set-up), with a median value of about 240. The full journal of observations is presented in Table 1.

Following Huélamo et al. (2008), we assume that the period of the RV variations is the rotation period. Rotational cycles E are computed from Heliocentric Julian Dates (HJD) according to the ephemeris (note the different initial HJD than that used by Huélamo et al. 2008):

$$\mathrm{HJD} = 245\,4540.0 + 3.5683E. \quad (1)$$

Coverage of the rotation cycle is only moderate in 2008 March (with a phase gap of about one-third of the cycle) and good in 2010 March (see Table 1). As a result of the difference in the assumed initial HJD, our rotation cycles are ahead of those of Huélamo et al. (2008) by 2.774 cycles (at both epochs); maximum RVs should thus occur around phase 0.1 in our ephemeris.

Least-squares deconvolution (LSD; Donati et al. 1997) was applied to all observations. The line list we employed for LSD is computed from an Atlas9 local thermodynamic equilibrium model atmosphere (Kurucz 1993) and corresponds to a K7V spectral type ($T_{\mathrm{eff}} = 4000$ K and $\log g = 4.5$) appropriate for TW Hya. Only moderate to strong atomic spectral lines (with line-to-continuum core depressions larger than 40 per cent prior to all non-thermal broadening) are included in this list; spectral regions with strong lines mostly formed outside the photosphere (e.g. Balmer, He, Ca II H, K and IRT lines) and/or heavily crowded with telluric lines were discarded. Altogether, about 6500 spectral features (with about 40 per cent from Fe I) are used in this process. Expressed in units of the unpolarized continuum level I_{c}, the average noise levels of the resulting Stokes V LSD signatures range from 1.9 to 6.4 $\times$ 10^{-4} per 1.8 km s^{-1} velocity bin (median value 2.4 $\times$ 10^{-4}). Zeeman

Downloaded from https://academic.oup.com/mnras/article/417/1/472/980080 by guest on 17 March 2022

Table 1. Journal of observations collected in 2008 March and 2010 March. Each observation consists of a sequence of four subexposures (each lasting 815 and 840 s in 2008 and 2010, respectively), except for the first three in 2008 March for which only two subexposures (of 815 s each) could be used (following an instrument set-up problem). Columns (1)–(4), respectively, list the UT date, the HJD and UT time (both at mid-exposure) and the peak S/N (per 2.6 km s^{-1} velocity bin) of each observation. Column (5) lists the rms noise level (relative to the unpolarized continuum level I_c and per 1.8 km s^{-1} velocity bin) in the circular polarization profile produced by LSD, while Column (6) indicates the orbital/rotational cycle associated with each exposure (using the ephemeris given by equation 1).

Date 2008	HJD (245 4500+)	UT (h:m:s)	S/N	σ_{LSD} ($10^{-4} I_c$)	Cycle (0+)
Mar 15	40.978 30	11:20:12	100	6.4	0.274
Mar 16	41.846 33	08:10:10	150	3.4	0.517
Mar 16	41.946 81	10:34:52	170	2.9	0.546
Mar 20	45.902 19	09:30:41	250	2.1	1.654
Mar 20	45.952 10	10:42:34	250	2.1	1.668
Mar 23	48.829 40	07:45:57	240	2.2	2.474
Mar 23	48.973 83	11:13:56	260	2.1	2.515
Mar 26	51.867 91	08:41:31	250	2.2	3.326
Mar 27	52.821 73	07:35:04	260	1.9	3.593
Mar 27	52.963 03	10:58:32	240	2.2	3.633
Mar 28	53.814 23	07:24:18	250	2.0	3.871
Mar 28	53.908 63	09:40:14	170	3.5	3.898
Mar 28	53.953 11	10:44:17	180	3.3	3.910
Date 2010	HJD (245 5200+)	UT (h:m:s)	S/N	σ_{LSD} ($10^{-4} I_c$)	Cycle (199+)
Feb 23	51.000 57	11:52:33	240	2.2	0.255
Feb 24	52.041 70	12:51:43	260	2.1	0.546
Feb 25	52.963 33	10:58:51	250	2.4	0.805
Feb 26	54.019 97	12:20:22	260	2.3	1.101
Feb 27	54.936 40	10:19:60	240	2.4	1.358
Feb 28	56.035 71	12:42:58	240	2.2	1.666
Mar 01	57.005 78	11:59:51	220	2.5	1.938
Mar 02	58.017 39	12:16:33	170	3.7	2.221
Mar 03	58.954 37	10:45:47	160	3.7	2.484
Mar 04	60.011 11	12:07:28	220	2.5	2.780
Mar 05	60.955 26	10:47:01	190	3.2	3.044
Mar 07	62.982 78	11:26:38	220	2.6	3.613
Mar 08	63.956 41	10:48:39	160	3.8	3.885

signatures are detected at all times in LSD profiles (see Fig. 2 for an example) and in most accretion proxies (see Section 4).

4 SPECTROSCOPIC VARIABILITY

In this section, we present a basic description of how the spectral lines of TW Hya, and in particular the photospheric LSD profiles and the selected accretion proxies [i.e. the Ca II IR triplet (IRT), the He I D_3 line and the first two lines of the Balmer series], vary with time and with rotation phase. The idea is to look at how the equivalent widths, the RVs and the average magnetic fluxes of the various profiles are modulated with rotation, to get a rough, intuitive understanding of how the large-scale field is structured and oriented, and how cool photospheric spots and hot chromospheric accretion regions are distributed over the stellar surface – to be compared with the results of the full tomographic imaging analysis carried out in the following section.

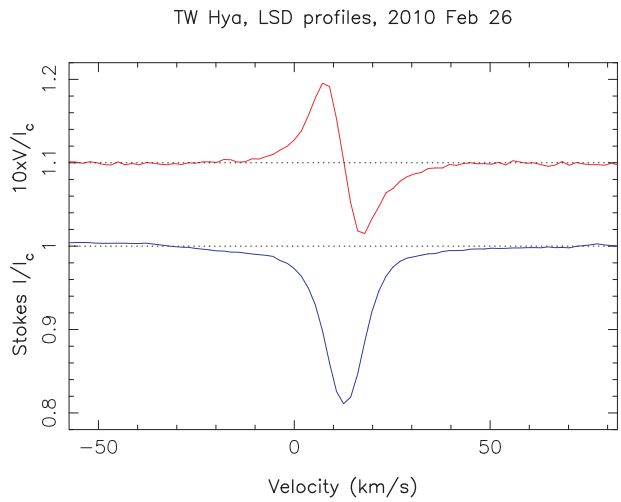

Figure 2. LSD circularly polarized (Stokes V) and unpolarized (Stokes I) profiles of TW Hya (top/red, bottom/blue curves, respectively) collected on 2010 February 26 (cycle 199+1.101). A strong Zeeman signature (with a full amplitude of 1.8 per cent) is detected in the LSD Stokes V profile, in conjunction with the unpolarized line profile. The mean polarization profile is expanded by a factor of 10 and shifted upwards by 1.1 for display purposes.

4.1 LSD photospheric profiles

As shown on Fig. 3 (top and middle panels), the photospheric Stokes I LSD profiles exhibit significant variability at the two observing epochs, both in position (RV) and strength (as a result of veiling).[1] Showing no more than a moderate level of intrinsic variability, RVs are clearly modulated by rotation, varying by $\simeq$0.5 km s^{-1} peak to peak around a mean of 12.55 $\pm$ 0.10 km s^{-1} and reaching a maximum at phase $\simeq$0.1 (corresponding to phase 0.88 in the ephemeris of Huélamo et al. 2008). This is fully compatible with the results of Huélamo et al. (2008), indicating that the RV variability we report is of the same origin and nature as that discussed by Huélamo et al. (2008), i.e. caused by a cool photospheric spot on TW Hya located at high latitudes and at phase $\simeq$0.35 (0.25 cycle after RV maximum); moreover, it suggests that this spot is apparently persistent on time-scales of at least 3 years.

LSD profiles of TW Hya are also significantly shallower than those expected from a standard star of similar spectral type, indicating that the spectrum is significantly veiled (as a likely result of accretion), at levels varying from 30 to 100 per cent (with an average of about 60 per cent). This is again typical to previously published reports (e.g. Yang et al. 2005). We find that veiling can be mainly modulated by rotation at times, as in 2008 March where maximum veiling is observed to occur at phase 0.6 (i.e. 0.25 cycle later than the phase at which the cool spot is best visible); at other times, veiling is dominated mostly by intrinsic variability, as in 2010 March where no clear trend with rotation phase is detected (see middle panels of Fig. 3).

As mentioned already, Zeeman signatures are detected at all times in Stokes V LSD profiles of TW Hya, showing a fairly canonical shape (i.e. antisymmetric with respect to the line centre) and an unusually large amplitude of almost 2 per cent peak to peak (see e.g.

[1] We assume a conservative error bar of $\pm$0.05 km s^{-1} and $\pm$2 per cent on the relative RV and the relative strength of photospheric LSD and Ca II IRT profiles; in particular, the error bar on the RVs of LSD profiles is larger than the formal error bar of 0.03 km s^{-1}, but comparable to the typical RV dispersion quoted by Huélamo et al. (2008).

© 2011 The Authors, MNRAS **417,** 472–487
Monthly Notices of the Royal Astronomical Society © 2011 RAS

Downloaded from https://academic.oup.com/mnras/article/417/1/472/980080 by guest on 17 March 2022

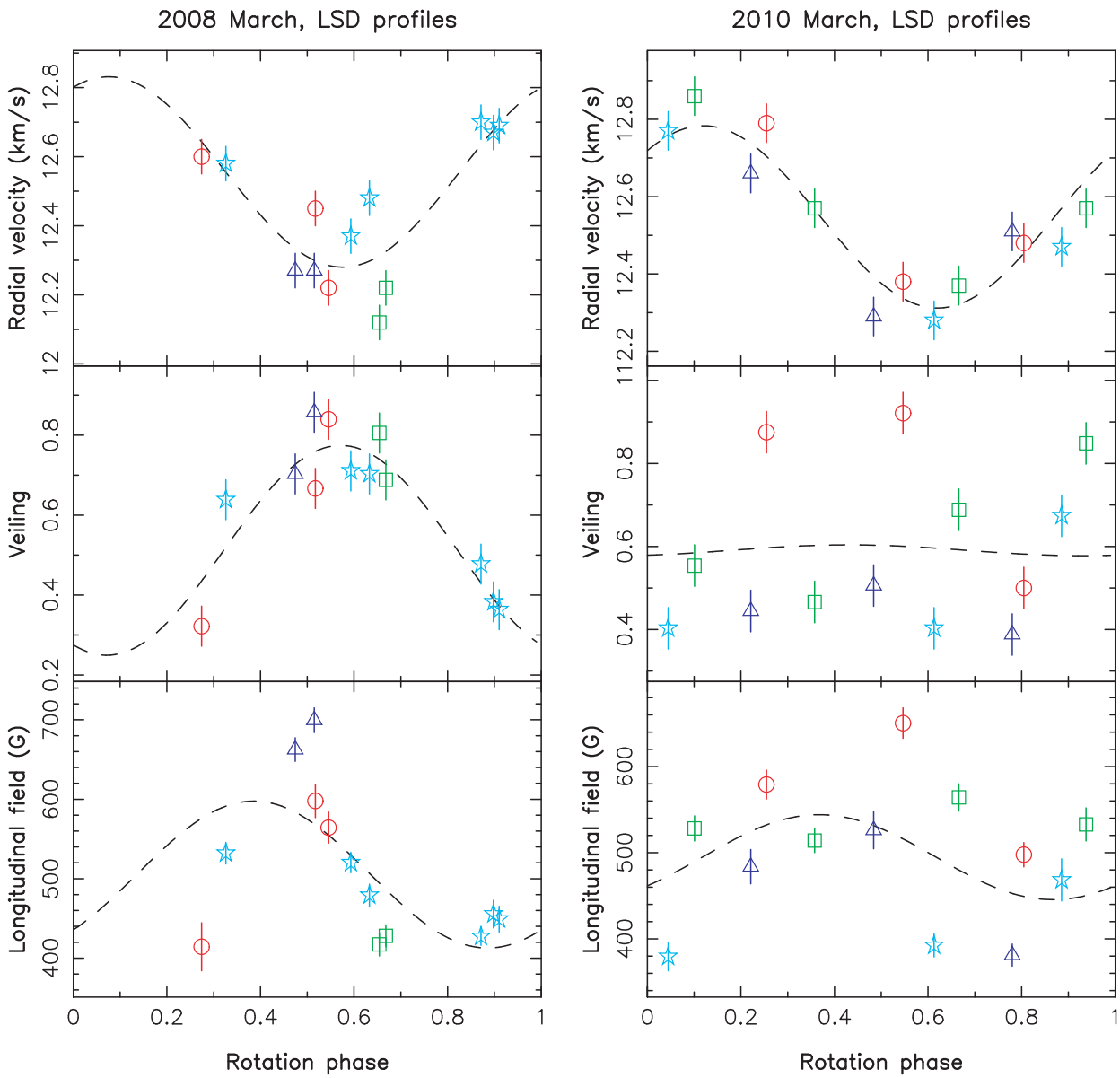

Figure 3. Rotational modulation of the RV (top row), veiling (second row) and longitudinal field (bottom row) derived from the LSD photospheric profiles of TW Hya in 2008 March (left-hand panels) and in 2010 March (right-hand panels). Data collected during rotational cycles 0, 1, 2 and 3 are, respectively, shown with red circles, green squares, dark blue triangles and light blue stars. Fits with sine/cosine waves are included (and shown as dashed lines) to outline (whenever significant) the amount of variability attributable to rotational modulation. $\pm 1\sigma$ error bars on data points are also shown.

Fig. 2). The line-of-sight projected component of the field averaged over the visible stellar hemisphere and weighted by brightness inhomogeneities (called the longitudinal field and estimated from the first moment of the Stokes V profile, e.g. Donati et al. 1997) ranges from 380 to 700 G, with typical error bars of $\simeq$15 G. Note that our longitudinal field estimates are significantly larger than those found in previously published studies (reporting values $\leq$150 G; Yang et al. 2007); this discrepancy can potentially be attributable to long-term evolution of the large-scale magnetic topology (as suggested for a similar mismatch in the case of the cTTS BP Tau; Donati et al. 2008b), as the data of Yang et al. (2007) were collected about a decade earlier than ours (in 1999).

As shown in Fig. 3 (bottom panels), the longitudinal field curves at both epochs include a significant amount of intrinsic variability (especially in 2010 March), but nevertheless suggest a $\pm$10–20 per cent level of rotational modulation about the mean value (of $\simeq$500 G), with maximum longitudinal field occurring at phase $\simeq$0.35, i.e. when the cool spot is best visible. Most likely, this intrinsic variability of the longitudinal field does not reflect a true change in the large-scale magnetic topology, but rather relates to modifications in the line formation region and related properties (e.g. veiling, cool spot location and size).

4.2 Ca II IRT emission

As in previous papers, we use core emission in Ca II IRT lines as our main proxy of surface accretion even though it usually features a significant contribution from the non-accreting chromosphere; previous work (e.g. Donati et al. 2010, 2011a) demonstrated in particular that rotational modulation in Stokes I and V Ca II IRT

Downloaded from https://academic.oup.com/mnras/article/417/1/472/980080 by guest on 17 March 2022

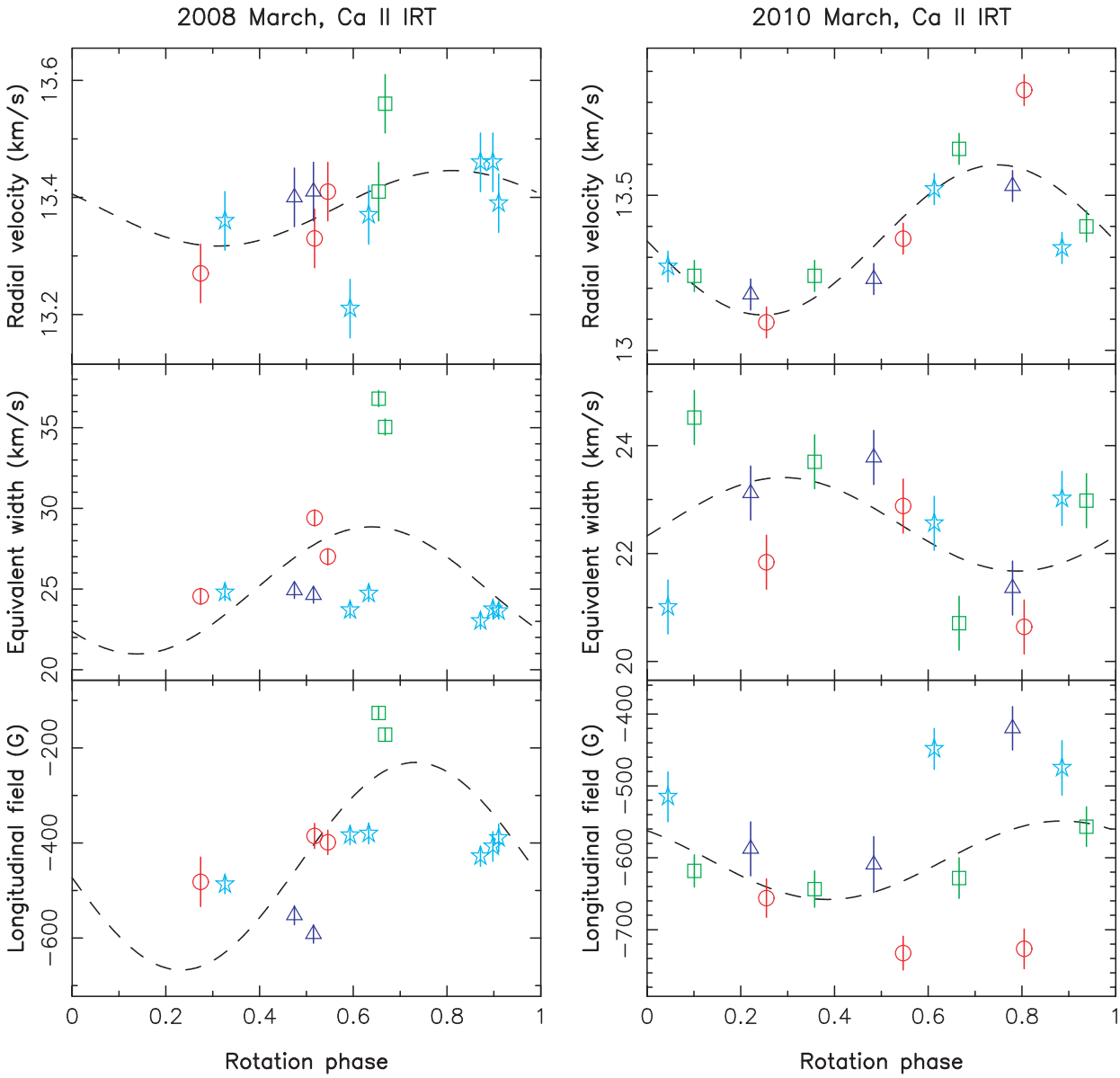

Figure 4. Same as Fig. 3 for the Ca II IRT LSD profiles.

profiles of cTTSs correlates well with that derived from the more conventional He I D_3 accretion proxy (see below), even at fairly low mass accretion rates. To recover the emission component of the Ca II IRT lines, we start by constructing a LSD-like weighted average of the three IRT lines; we then subtract the underlying (much wider) photospheric absorption profiles, with a single Lorentzian fit to the far line wings (see Donati et al. 2011b, for an illustration).

The average Ca II emission profiles are centred at a RV of $\simeq$13.40 km s^{-1}, i.e. slightly redshifted (by 0.85 km s^{-1}) with respect to the photospheric LSD profiles (see Fig. 4, top panels); this is usual for cTTSs and further confirms that Ca II emission probes slowly moving plasma in the post-shock regions of accretion funnels, and located close to the surface of the star. We also observe that the RVs of the Ca II emission profiles show, in addition to a weak level of intrinsic variability, a small amount of rotational modulation, with an amplitude comparable to (in 2010 March) or smaller than (in 2008 March) that seen in the LSD photospheric profiles and much smaller (by at least a factor of 15) than the rotational broadening of spectral lines ($v \sin i \simeq 4$ km s^{-1}; see Section 5). It suggests in particular the presence of a localized region of accretion-powered emission near the pole, and best viewed (at both epochs) at a rotational phase of $\simeq$0.5 (i.e. at mid-transit between minimum and maximum RVs). This approximately coincides with the phase of maximum veiling in 2008 March ($\simeq$0.6; see above) and with that at which the cool photospheric spot (probed through LSD profiles) is best visible ($\simeq$0.35), the associated phase shifts (of +0.10 and –0.15 rotation cycle, respectively) being not necessarily very significant at high latitudes and with such a high level of intrinsic variability.

Emission strength is also varying with time (see middle panels of Fig. 4), with equivalent widths typically within the range 20–30 km s^{-1} (0.055–0.085 nm) and featuring at times short-lived sporadic bursts during which emission is temporarily enhanced by as much as 50 per cent (e.g. at cycles 1.654 and 1.668 in 2008 March). Rotational modulation is moderate, potentially up to 30 per cent peak to peak in 2008 March, with maximum emission occurring near phase 0.6 (in conjunction with the phase of maximum

Downloaded from https://academic.oup.com/mnras/article/417/1/472/980080 by guest on 17 March 2022

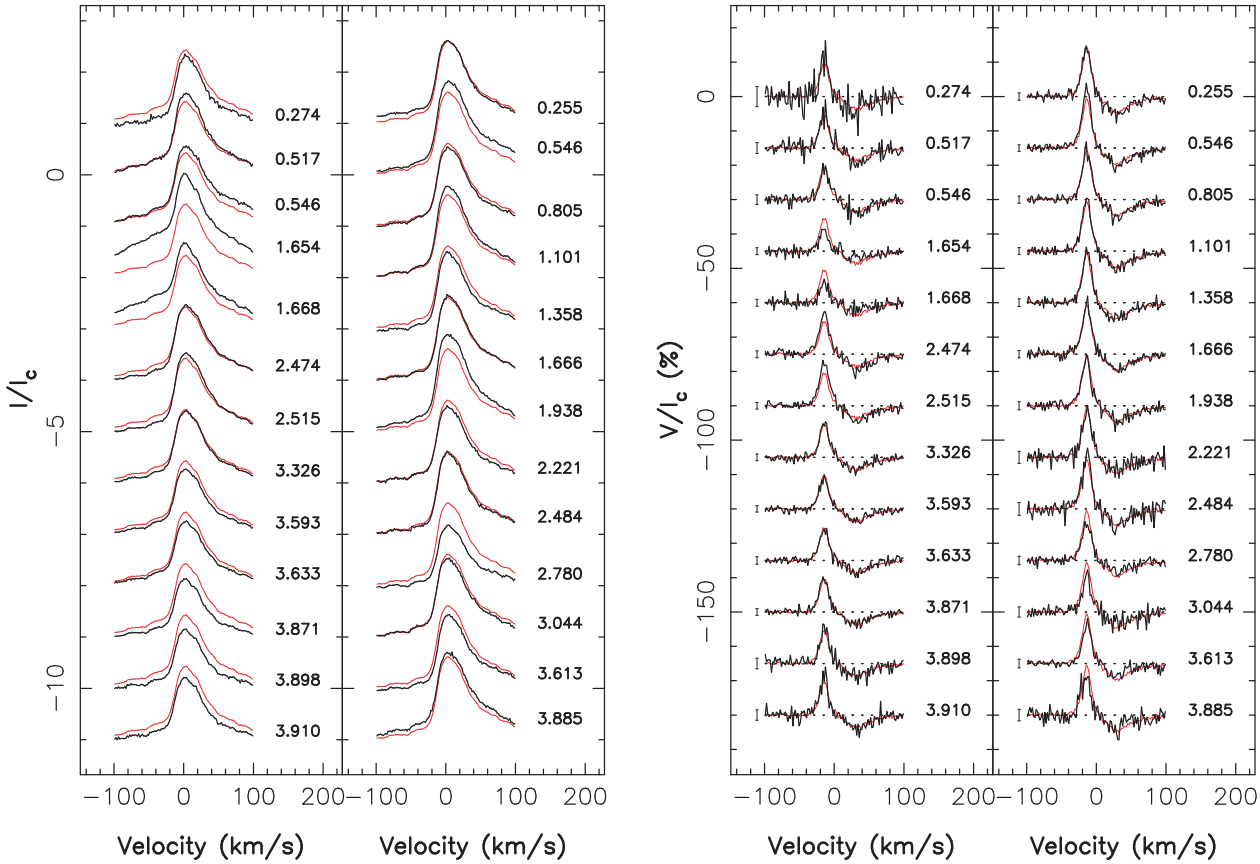

Figure 5. Variations of the unpolarized (Stokes I, left-hand panel) and circularly polarized (Stokes V, right-hand panel) profiles of the He I D_3 emission of TW Hya in 2008 March (left-hand columns of both panels) 2010 March (right-hand columns). The unpolarized emission profile is asymmetric with respect to the line centre and can be described as the sum of a central narrow component and a broad (often red-shifted) component (see text). A strong Zeeman signature (with a full amplitude of $\simeq$20 per cent) is detected in conjunction with the central narrow He I emission, but not with the broad redshifted component. To emphasize variability, the average profile over each run is shown in red. Rotation cycles (as listed in Table 1) and 3σ error bars (for Stokes V profiles only) are shown next to each profile.

veiling; see above); in 2010 March, however, rotational modulation is much lower (lower than 10 per cent peak to peak) and mostly hidden by intrinsic variability.

As for LSD profiles, clear Zeeman signatures are detected at all times in conjunction with the emission component of Ca II IRT lines, with peak-to-peak amplitudes reaching up to 10 per cent (in 2010 March). The corresponding longitudinal fields range between −380 and −730 G (with typical error bars of about 30 G), except during the previously mentioned emission burst (when the longitudinal field is reduced to −150 G). Note in particular the striking polarity contrast between the (constantly negative) longitudinal fields measured from the Ca II emission lines and those (always positive) derived from the LSD profiles; this clearly demonstrates that LSD profiles and IRT lines probe different areas (of different magnetic polarities) over the stellar surface of TW Hya (as on V2129 Oph and BP Tau; Donati et al. 2011a, 2008b). The field values we derive from the Ca II IRT profiles are comparable (both in strength and sign) to those reported in a previous paper (Yang et al. 2007), in contrast to longitudinal fields from LSD photospheric profiles (found to be significantly stronger in our study; see above); it may suggest that the potential field evolution between the two studies concerns the magnetic topology as a whole and not just its overall strength.

Again, intrinsic variability is dominant at both epochs, and no more than a moderate level of rotational modulation is observed, with strongest longitudinal fields occurring approximately when the cool photospheric spot is best visible (i.e. around phase 0.35); as for longitudinal fields estimated from LSD profiles, we suggest that this intrinsic variability reflects changes in the line formation region (and in particular in the accretion region) rather than in the large-scale magnetic topology itself.

4.3 He I D_3 emission

The He I D_3 line, used in most cases as the reference accretion proxy, exhibits, in the spectrum of TW Hya, an emission profile that is strongly asymmetric with respect to the line centre (see Fig. 5). This profile can be decomposed into a narrow central emission centred at $\simeq$18.2 km s^{-1} (i.e. redshifted by about 5.6 km s^{-1} with respect to the LSD profiles) and whose full width at half-maximum is $\simeq$36 km s^{-1}, and a broad emission component (full width at half-maximum $\simeq$110 km s^{-1}) redshifted by typically 20–30 km s^{-1} with respect to the narrow component; the equivalent width of the narrow component (35 and 45 km s^{-1} on average in 2008 March and 2010 March, respectively, or equivalently 0.07 and 0.09 nm) is about half that of the broad component ($\simeq$75 km s^{-1} or 0.15 nm). Zeeman signatures with typical amplitudes of $\simeq$20 per cent are observed in conjunction with the narrow emission component, but not with the broad component (see Fig. 5). Their shape strongly departs from the usual antisymmetric pattern (with respect to the line centre), likely indicating that the line forms in a region with significant

Downloaded from https://academic.oup.com/mnras/article/417/1/472/980080 by guest on 17 March 2022

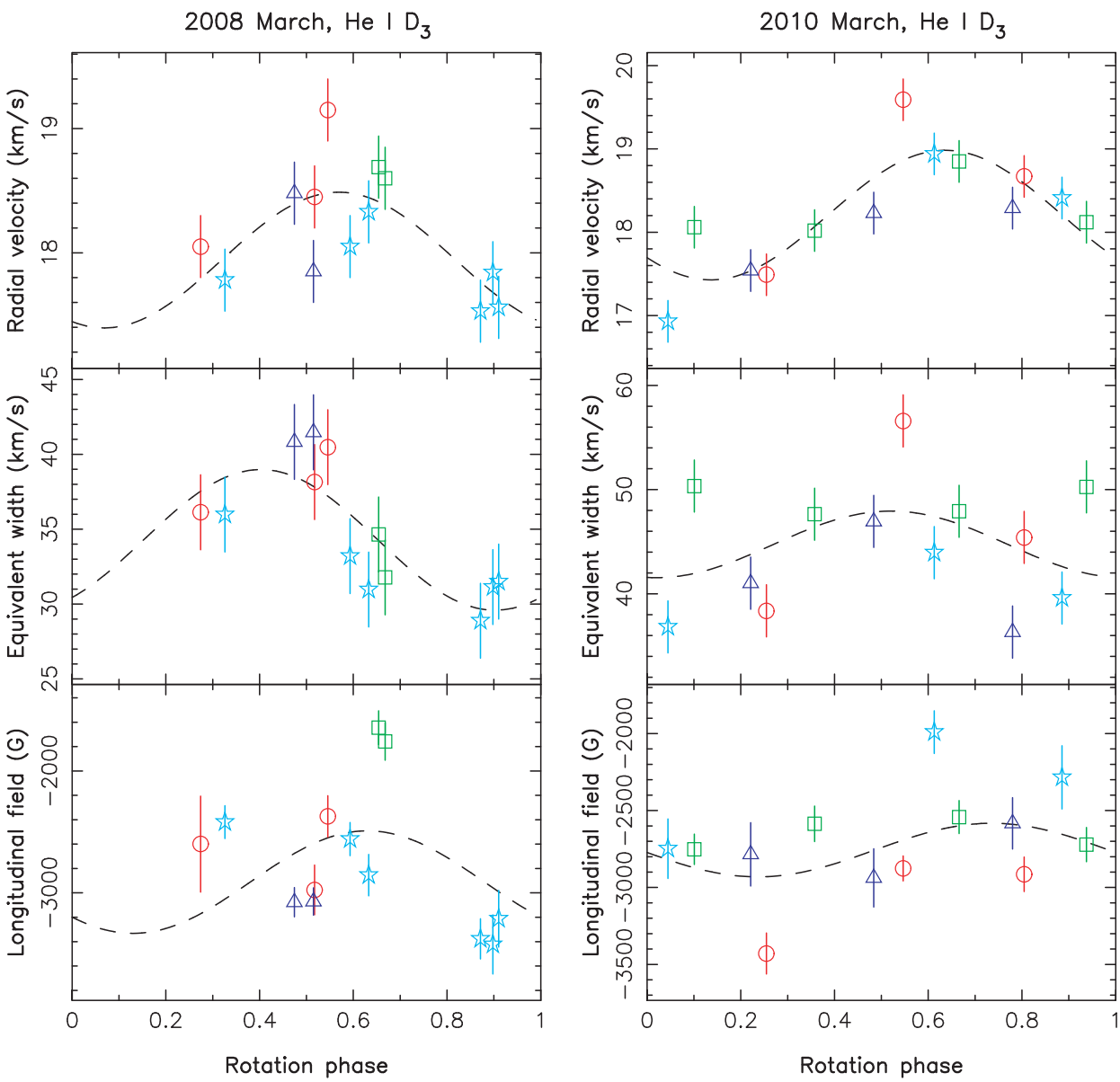

Figure 6. Same as Fig. 3 for the narrow component of the He I D_3 profiles.

velocity gradients (e.g. Sanchez Almeida & Lites 1992). We suggest that this narrow emission component comes from the post-shock region in which the post-shock plasma is strongly decelerating though still falling towards the stellar surface (hence the redshifted emission and the non-antisymmetric Zeeman signature). Similarly, we propose that the broad emission component probes the whole accretion funnels rather than just the post-shock region (hence the larger linewidth and redshift, reflecting the higher plasma velocities involved). In the following, we focus on the narrow emission component mostly, being the most relevant one for our study on the large-scale field topology, photospheric spots and accretion regions at the surface of TW Hya.

The temporal variability of the narrow He I emission is shown in Fig. 6 for both observing epochs.[2] We find that the RV of the narrow He I emission is modulated by rotation in a similar way to that of the Ca II IRT emission, suggesting again the presence of an accretion region located around phase 0.3–0.4 (at mid-distance between minimum and maximum RVs), i.e. more or less cospatial with the cool photospheric spot probed through LSD profiles (see above). The semi-amplitude of the RV variations reaches 0.5–0.8 km s^{-1} for the narrow He I emission (see Fig. 6, top panels), significantly larger than those seen in the Ca II IRT lines; this is in agreement with the much smaller dilution that the He I line suffers from the non-accreting chromosphere. Assuming that this dilution is negligible for the He I line and thus that the associated RV fluctuations directly track the Doppler motion of the hotspot, we infer that this accretion region is off-centred with respect to the pole by typically 10° (for $v \sin i = 4$ km s^{-1}).

[2] We assume an error bar of ±0.25 and ±2.5 km s^{-1} on the relative RV and the relative strength of the narrow He I emission component, i.e. five times larger than those used for the Ca II IRT profiles to reflect the reduced accuracy resulting from the subtraction of the broad He I emission component.

© 2011 The Authors, MNRAS **417,** 472–487
Monthly Notices of the Royal Astronomical Society © 2011 RAS

Downloaded from https://academic.oup.com/mnras/article/417/1/472/980080 by guest on 17 March 2022

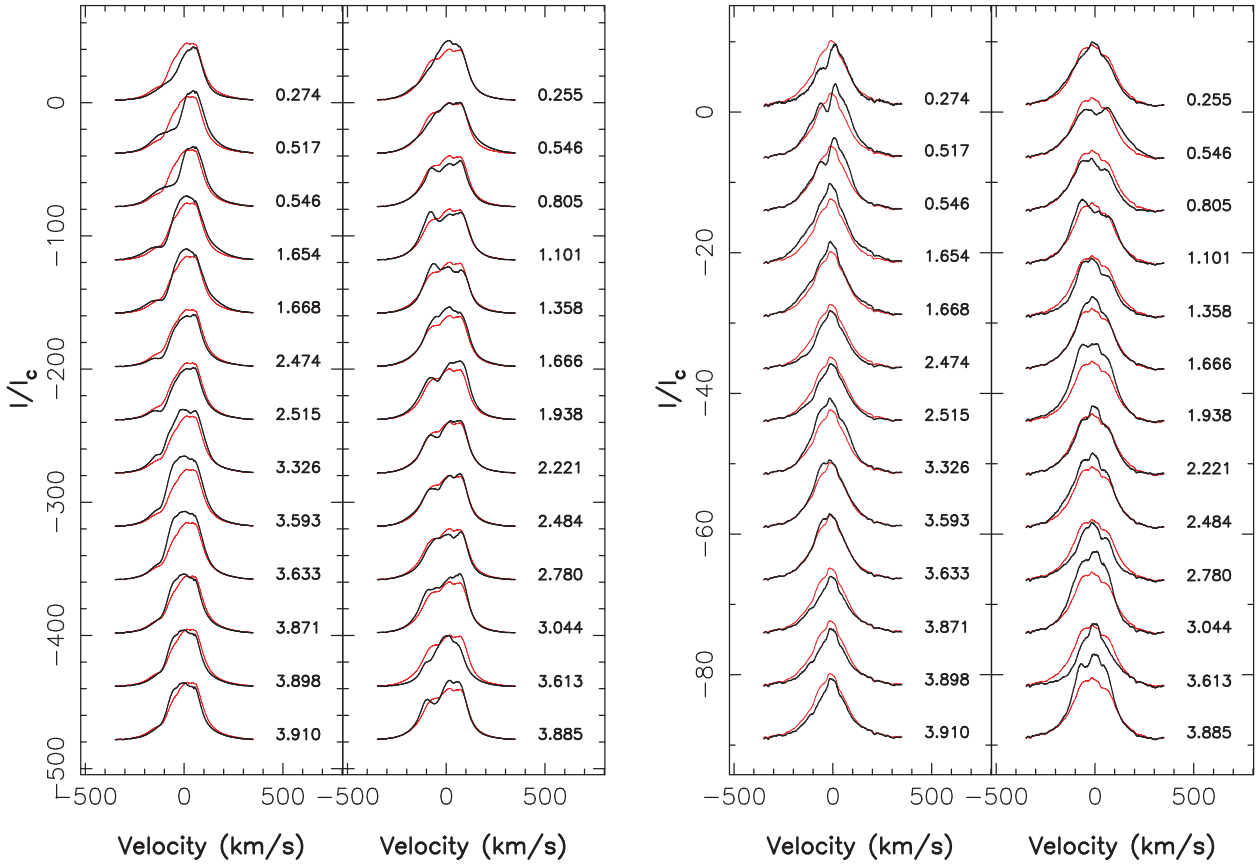

Figure 7. Variations of the Hα (left-hand panel) and Hβ (right-hand panel) lines in the spectrum of TW Hya, in 2008 March (left-hand column of both panels) and 2010 March (right-hand columns). To emphasize variability, the average profile over each run is shown in red. Rotation cycles (as listed in Table 1) are mentioned next to each profile.

We also find that the equivalent width of the narrow He I emission is varying with time. Rotational modulation is again moderate, up to about 30 per cent and peaking at phase $\simeq$0.4 in 2008 March and no larger than 10 per cent in 2010 March (see Fig. 6, middle panels); intrinsic variability is significant and dominates in 2010 March. These conclusions mostly confirm what the Ca II IRT lines already suggested (see above). Surprisingly, the emission burst detected in Ca II does not seem to show up in the narrow He I emission component, although clearly detected in the He I line (broad component); this may, however, reflect the limits of our two-component decomposition (used to describe the He I line) in the particular case of emission bursts (where both components happen to have roughly equal RVs; see Fig. 5).

The longitudinal fields we derive from the observed Zeeman signatures range from -2 to -3.5 kG (see Fig. 6, bottom panels) when we take into account that the narrow He I emission is the only contributor. Unsurprisingly, the field polarity is the same as that derived from Ca II IRT emission, demonstrating that both lines are reliable probes of accretion regions (even though Ca II emission suffers a strong dilution from the non-accreting chromosphere). Our He I longitudinal field estimates are significantly larger than those of Yang et al. (2007) by typically a factor of 2; this discrepancy is, however, only apparent and reflects their assumption that the full He I emission (including the broad emission, rather than the narrow component only) contributes to the Zeeman signatures.

As for the Ca II IRT emission, intrinsic variability dominates and only moderate rotational modulation is observed, with maximum longitudinal field (of about -3 kG) occurring approximately when the cool photospheric spot is best visible; once again, we suspect that frequent changes in the properties of the accretion region are causing the enhanced dispersion of the observed longitudinal fields.

4.4 Balmer emission

Balmer lines are also strongly in emission in the spectrum of TW Hya, with Hα and Hβ reaching typical equivalent widths of 8000–10 000 km s^{-1} (18–22 nm) and 1700–2100 km s^{-1} (2.8–3.4 nm), respectively. At times, they show a conspicuous blueshifted absorption component (e.g. at cycles 0.274–0.546 in 2008 March), indicating the presence of a strong wind escaping the star at an average projected velocity of $\simeq$50 km s^{-1}.

Both lines exhibit significant fluctuations with time (see Fig. 7); however, since the profiles and emission strengths of Hα and Hβ do not convincingly repeat between consecutive rotation cycles (e.g. cycles 0.517 and 2.515 in 2008 March, cycles [199+] 0.255 and 2.221 in 2010 March), these variations cannot be attributed to rotational modulation and are more likely caused by intrinsic temporal evolution of the accretion and wind flows. In 2008 March, the blueshifted wind absorption is causing most of the observed variability in Hα and Hβ; in 2010 March, the emission fluxes of both Balmer lines correlate well with that of the broad (and not of the narrow) He I emission component.

We also note that the red wing of Hβ is depressed at times with respect to the average profile (e.g. at cycle [199+] 0.805 in

Downloaded from https://academic.oup.com/mnras/article/417/1/472/980080 by guest on 17 March 2022

2010 March). However, these depressions never show up as true absorption as they regularly do on some cTTSs (e.g. AA Tau and V2129 Oph; Bouvier et al. 2007b; Donati et al. 2011a); we thus think it is ambiguous and potentially misleading to relate these events to the crossing of accretion funnels in front of the visible hemisphere of TW Hya (as done for AA Tau and V2129 Oph), as they could just as well result from varying projection effects of the magnetospheric funnel structure.

4.5 Mass accretion rate

From the average equivalent widths of the Ca II IRT, He I (narrow component) and Hβ lines, we can derive logarithmic line fluxes (with respect to the luminosity of the Sun $L_\odot$), equal to -4.8, -4.8 and -3.3, respectively,[3] implying logarithmic accretion luminosities (with respect to $L_\odot$) of -2.1, -1.6 and -1.2, respectively (using empirical correlations from Fang et al. 2009). We thus conclude that the average logarithmic mass accretion rate of TW Hya (in $M_\odot\ yr^{-1}$) is equal to -8.9 ± 0.4 at both epochs, in rough agreement with the estimate of Curran et al. (2011), equal to -9.2 ± 0.2 and also derived from optical lines (though from fully independent data and a different analysis).

Mass accretion rates can in principle also be estimated (though less accurately) through the full width of Hα at 10 per cent height (e.g. Natta et al. 2004; Cieza et al. 2010). In the case of TW Hya, Hα shows a full width of $\simeq$400 km s^{-1} on average, implying a logarithmic mass accretion rate estimate of -9.0 ± 0.6 (in $M_\odot\ yr^{-1}$) in agreement with our previous estimate.

5 MAGNETIC MODELLING

5.1 Overview of the method

Now that the temporal variability of photospheric LSD and Ca II IRT emission profiles has been examined in detail, we aim at converting the corresponding data sets into maps of the large-scale magnetic topology, as well as distributions of surface cool spots and of chromospheric accretion regions, at the surface of TW Hya. To achieve this, we apply our tomographic imaging technique, described extensively in previous similar studies (e.g. Donati et al. 2010, 2011a).

Following the principles of maximum entropy, our code automatically and simultaneously derives the simplest magnetic topology, photospheric brightness image and accretion-powered Ca II emission map compatible with the series of observed Stokes *I* and *V* LSD and Ca II IRT profiles. The reconstruction process is iterative and proceeds by comparing at each step the synthetic Stokes *I* and *V* profiles corresponding to the current images with those of the observed data set. The magnetic topology is described through its poloidal and toroidal components expressed as spherical-harmonics (SH) expansions (e.g. Donati et al. 2006). The spatial distributions of photospheric brightness (with respect to the quiet photosphere) and those of accretion-powered Ca II emission (in excess of and with respect to that produced by the quiet chromosphere) are modelled as series of independent pixels (typically a few thousand) on a grid covering the visible surface of the star (with spots in the brightness image assumed to be darker/cooler than the quiet photosphere and accreting regions in the Ca II emission maps supposed to be brighter than the quiet chromosphere).

Synthetic profiles are computed by summing up the elementary spectral contributions from all image pixels over the visible stellar hemisphere, taking into account the relevant local parameters of the corresponding grid cells (e.g. brightness, accretion-powered excess emission, magnetic field strength and orientation, RV, limb angle, projected area). Since the problem is partly ill-posed, we stabilize the inversion process by using an entropy criterion (applied to the SH coefficients and to the brightness/excess emission image pixels) aimed at selecting the magnetic topology and images with minimum information among all those compatible with the data. The relative weights attributed to the various SH modes can be imposed, e.g. for purposely producing antisymmetric or symmetric field topologies with respect to the centre of the star (by favouring odd or even SH modes; Donati et al. 2007, 2008b). More details concerning the specific description of local profiles used in the model can be found in Donati et al. (2010).

5.2 Application to TW Hya

Our imaging model assumes that the observed profile variations are mainly due to rotational modulation; all other sources of profile variability (and in particular intrinsic variability) cannot be properly reproduced and thus contribute as noise into the modelling process, degrading the imaging performance and potentially even drowning all relevant information. Filtering out significant intrinsic variability from the observed profiles is thus worthwhile to optimize the behaviour and convergence of the imaging code.

We implement this by applying specific corrections on our data set. We first suppress veiling by scaling all LSD Stokes *I* and *V* photospheric profiles to ensure that unpolarized lines have the same equivalent widths. We also remove the non-rotationally modulated part in the observed fluctuations of Ca II IRT emission by fitting them with a sine+cosine wave (see Fig. 8) and by scaling the corresponding Stokes *I* and *V* profiles accordingly, thus ensuring that equivalent widths of unpolarized lines match the optimal fit. Although only approximate (especially the removal of the intrinsic variability), this procedure is at least straightforward and has proved successful when applied to real data (e.g. Donati et al. 2011a) and efficient at retaining rotational modulation mostly. In the particular case of the present data set, the most significant effect of this filtering process is to remove the emission burst detected in 2008 March (at cycles 1.654 and 1.668) by scaling down the two corresponding Ca II IRT profiles (shown as green open squares in Fig. 8, left-hand panel); the remaining modulation left in the Ca II profiles are the $\simeq$30 and $<$10 per cent fluctuations reported in Section 4.

We use Unno–Rachkovsky's equations known to provide a good description of the local Stokes *I* and *V* profiles (including magneto-optical effects) in the presence of both weak and strong magnetic fields (e.g. Landi degl'Innocenti & Landolfi 2004; Section 9.8) despite their being based on the assumption of a simple Milne–Eddington atmospheric model. The model parameters used in the specific case of TW Hya are mostly identical to those used in our previous studies (Donati et al. 2010, 2011a). The emission profile scaling factor ϵ, describing the emission enhancement of accretion regions over the quiet chromosphere, is once again set to $\epsilon = 10$. We also assume (as in previous studies) that the magnetic topology of TW Hya is antisymmetric with respect to the centre of the star; such field configurations are indeed best suited to explain how accretion regions can form at high latitudes mostly (e.g. Long, Romanova & Lovelace 2008), as often is the case for cTTSs. This assumption has

[3] To derive line fluxes from normalized equivalent widths, we approximate the continuum level by a Planck function at the temperature of the stellar photosphere.

© 2011 The Authors, MNRAS **417,** 472–487
Monthly Notices of the Royal Astronomical Society © 2011 RAS

Downloaded from https://academic.oup.com/mnras/article/417/1/472/980080 by guest on 17 March 2022

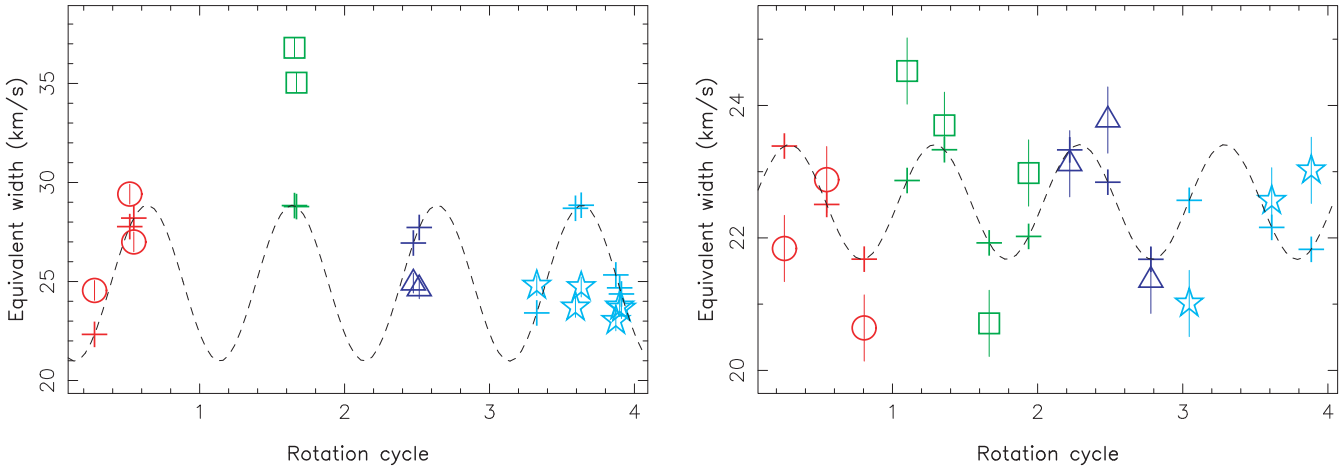

Figure 8. Measured (open symbols) and fitted (plus symbols) equivalent widths of the Ca II IRT LSD profiles of TW Hya in 2008 March (left-hand panel) and 2010 March (right-hand panel). The model wave (dashed line) providing the best (sine+cosine) fit to the data presumably traces rotational modulation, while the deviation from the fit illustrates the strength of intrinsic variability. The open symbols are defined as described in Fig. 3.

little impact on the reconstructed magnetic maps over the visible regions of the stellar surface and allows a consistent and realistic (though not necessarily exact) field distribution to be recovered on the unseen hemisphere as well.

The magnetic, brightness and accretion maps we reconstruct for TW Hya at both epochs are shown in Fig. 9, with the corresponding fits to the data shown in Fig. 10. The SH expansion describing the field was limited to terms with $\ell \leq 5$; attempts with $\ell = 10$ indicate that little power is reconstructed in higher order modes ($\ell \geq 6$), reflecting essentially the limited spatial information accessible to Doppler tomography at low $v \sin i$ values. Error bars on Zeeman signatures were artificially expanded by a factor of 3 (for LSD profiles) and 2 (for Ca II emission) at both epochs to take into account the significant level of intrinsic variability; moreover, Zeeman signatures corresponding to the two Ca II profiles recorded during the emission burst of 2008 March (at cycles 1.654 and 1.668) were excluded from the fit, being strongly discrepant with others taken at very similar phases (but different cycles, e.g. 3.633). The fits we finally obtain correspond to a reduced chi-square $\chi^2_{\rm r}$ of 1.2, starting from initial values of 59 and 47 for the 2008 March and 2010 March data sets, respectively (with scaled-up error bars on Zeeman signatures).

As a by-product, we obtain new estimates for various spectral characteristics of TW Hya; in particular, we find that the RV is equal to 12.55 ± 0.10 km s^{-1}, that the mean redshift of Ca II emission profiles with respect to LSD profiles is 0.85 ± 0.1 km s^{-1} and that the $v \sin i$ is 4 ± 1 km s^{-1}. Finally, we find that the profiles are best fitted for a value of the local filling factor ψ, describing the relative proportion of magnetic areas at any given point of the stellar surface, equal to $\simeq$0.4.

5.3 Modelling results

The reconstructed large-scale magnetic topology of TW Hya is very similar at both epochs, featuring a strong and mostly axisymmetric field as expected from the small amount of rotational modulation that Zeeman signatures exhibit. The magnetic field at the surface of the star has an average intensity of $\simeq$1.5 kG, concentrating mostly in the radial and meridional components; in particular, the radial field map consists of a spot of negative radial field near the pole (where the field reaches up to 3 kG, in agreement with the field strengths estimated from the narrow He I emission component) surrounded with a ring of positive radial field at low latitudes (see Fig. 9). We find that the field is almost purely poloidal and mostly axisymmetric at both epochs, with $\leq$5 per cent of the reconstructed magnetic energy in the toroidal and non-axisymmetric (i.e. SH modes with $m > \ell/2$) poloidal fields.

The octupolar component of the poloidal field largely dominates at both epochs (reaching polar strengths of 2.5 and 2.8 kG in 2008 March and 2010 March, respectively) as expected from the topologies of the reconstructed radial and meridional field maps; the dipole component is typically four to six times weaker, with a polar strength of 0.4 and 0.7 kG in 2008 March and 2010 March, respectively. The octupole is aligned with respect to the rotation axis to better than 10°, with the negative pole being visible from the Earth. The reconstructed dipole component is also aligned with the rotation axis in 2010 March but tilted by about 45° (towards phase 0.5) in 2008 March. However, given the relative weakness of the dipole field and the incomplete phase coverage of the data set at this epoch, it is unclear whether this tilt is significant; extensive simulations indeed suggest that retrieving a weak dipole component in a predominantly octupolar large-scale field is uncertain, especially at low $v \sin i$ values. At both epochs, the visible pole of the dipolar component is the positive pole, suggesting that the dipole and octupole components are essentially antiparallel in 2010 March. Given the high level of intrinsic variability in the data, we caution that the (limited) change in the large-scale magnetic topology of TW Hya (especially regarding the dipole component) between the two epochs may potentially be spurious.

The brightness distributions at the surface of TW Hya that we recover show a cool spot near the pole at both epochs (see Fig. 9). This spot, covering about 2 per cent of the stellar surface, is shifted from the pole by about 10° towards phase 0.35–0.40, as expected from the RV variations of photospheric LSD profiles (see Section 4). This spot is located right on the region of strong negative radial field near the pole (the magnetic pole of the octupole component), explaining a posteriori why photospheric Zeeman signatures are essentially insensitive to this strong negative radial field region and probe instead fields of opposite polarities (positive radial and meridional fields at intermediate latitudes; see Fig. 9); being very cool, this spot emits much less photons (per surface area) than the surrounding photosphere and therefore much less polarized photons

Downloaded from https://academic.oup.com/mnras/article/417/1/472/980080 by guest on 17 March 2022

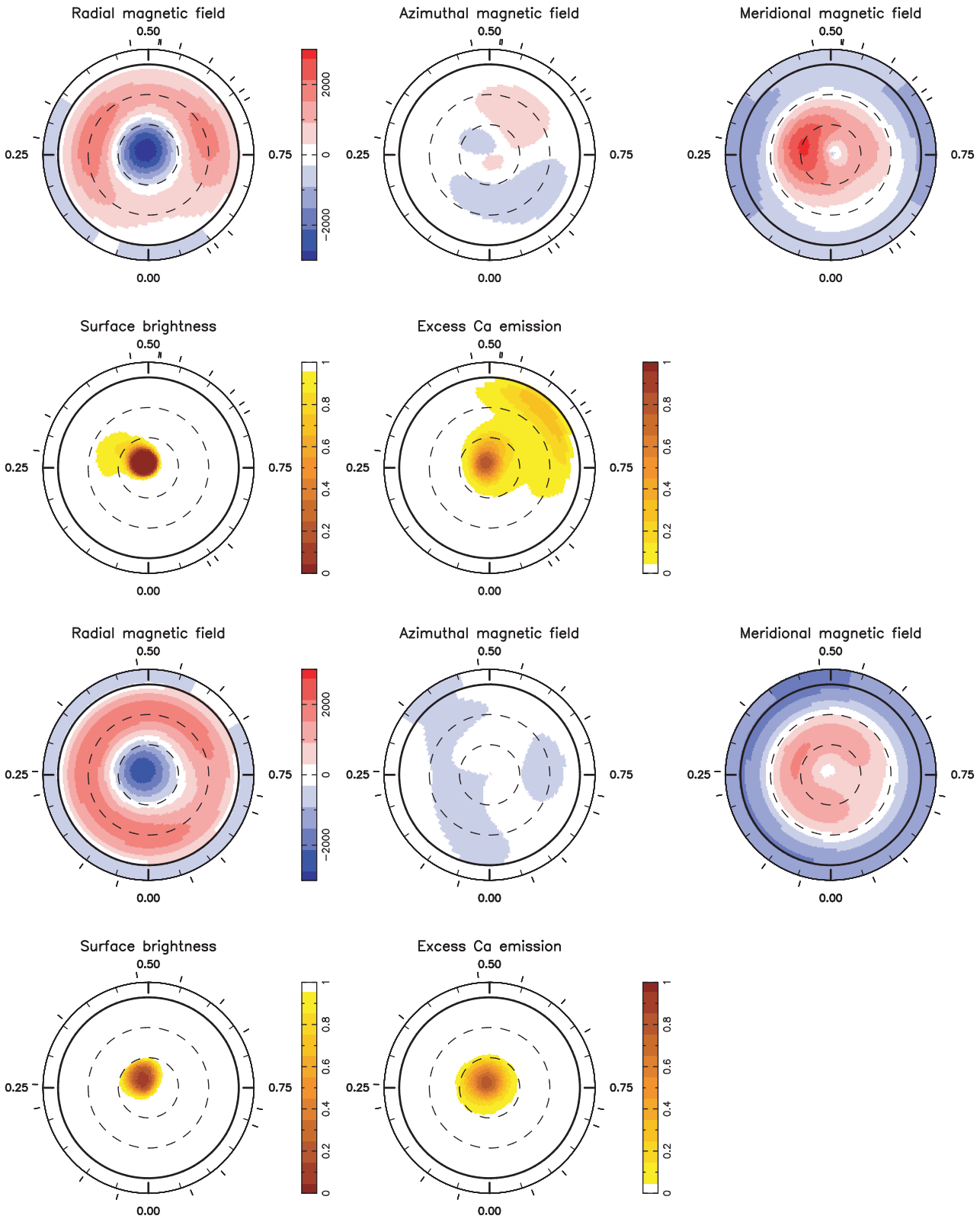

Figure 9. Maps of the radial, azimuthal and meridional components of the magnetic field $\boldsymbol{B}$ (first and third rows, left- to right-hand panels, respectively), photospheric brightness and excess Ca II IRT emission (second and fourth rows, first and second panels, respectively) at the surface of TW Hya, in 2008 March (top two rows) and 2010 March (bottom two rows). Magnetic fluxes are labelled in G; local photospheric brightness (normalized to that of the quiet photosphere) varies from 1 (no spot) to 0 (no light); local excess Ca II emission varies from 0 (no excess emission) to 1 (excess emission covering 100 per cent of the local grid cell, assuming an intrinsic excess emission of 10 times the quiet chromospheric emission). In all panels, the star is shown in flattened polar projection down to latitudes of $-30°$, with the equator depicted as a bold circle and parallels as dashed circles. Radial ticks around each plot indicate phases of observations.

Downloaded from https://academic.oup.com/mnras/article/417/1/472/980080 by guest on 17 March 2022

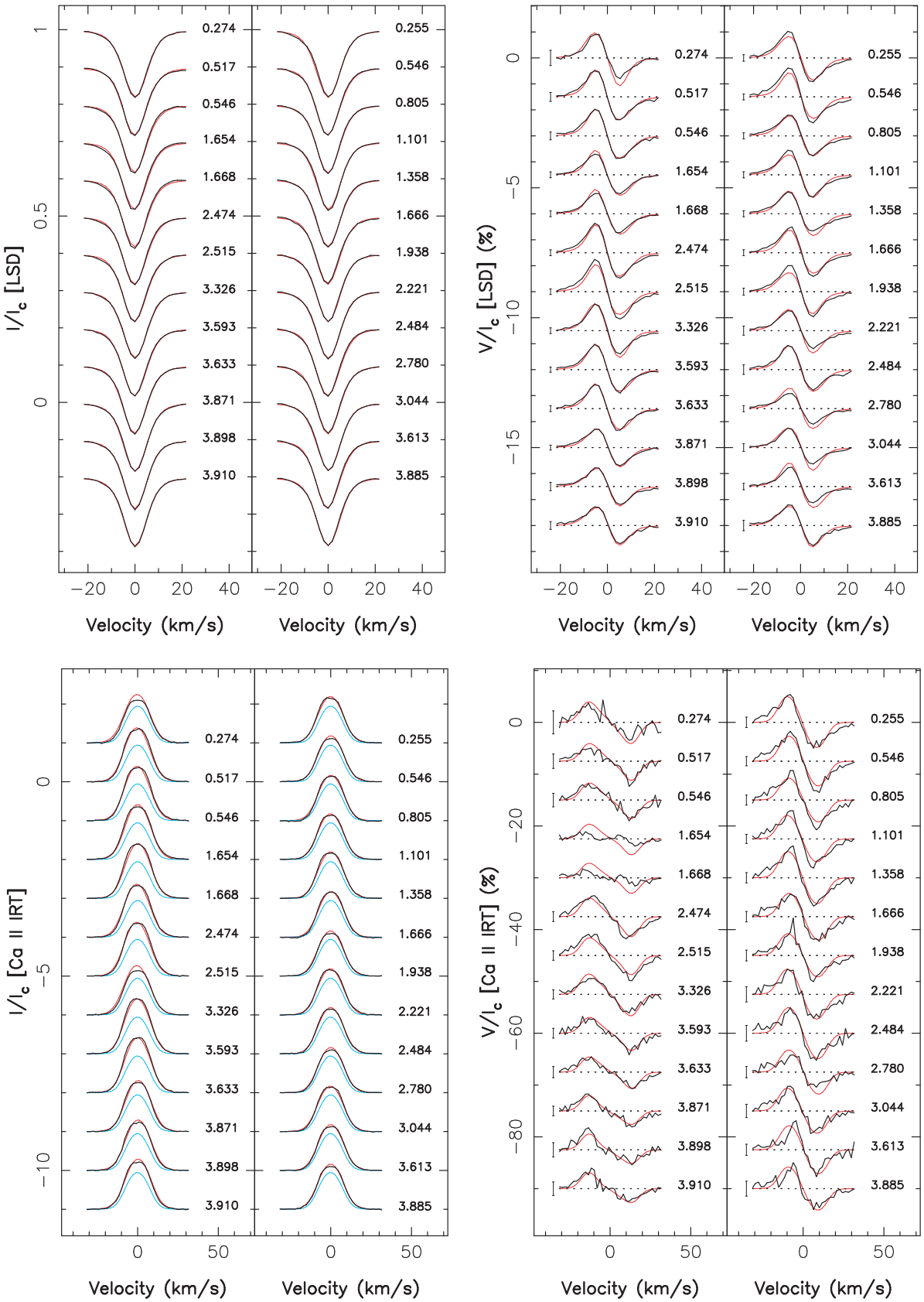

Figure 10. Maximum-entropy fit (thin red line) to the observed (thick black line) Stokes *I* and *V* LSD photospheric profiles (top panels) and Ca II IRT profiles (bottom panels) of TW Hya. In each panel, the left- and right-hand columns correspond to the 2008 March and 2010 March data, respectively. The light blue curve in the bottom left-hand panel shows the (constant) contribution of the quiet chromosphere to the Stokes *I* Ca II profiles. Rotational cycles and 3σ error bars (for Stokes *V* profiles) are also shown next to each profile (the two profiles with no error bars were excluded from the fit).

Downloaded from https://academic.oup.com/mnras/article/417/1/472/980080 by guest on 17 March 2022

as well, making it essentially invisible to Zeeman signatures of photospheric LSD profiles (at least at visible wavelengths).

The distributions of accretion-powered excess emission also show at both epochs a clear spot near the pole, and covering 2–3 per cent of the stellar surface (see Fig. 9). This accretion region approximately overlaps with the cool photospheric spot, with possibly a small phase shift (towards phase 0.50 in 2010 March in particular) suggesting that the accretion region may slightly trail the photospheric spot. These distributions explain a posteriori why Zeeman signatures of Ca II (and He I) emission profiles mostly probe fields with a polarity opposite to those traced by LSD photospheric profiles; while Ca II (and to a much larger extent He I) emission profiles are mostly sensitive to the polar regions (hosting strong negative radial fields), LSD photospheric profiles provide a complementary view of the visible stellar surface (and in particular of intermediate latitude regions, hosting positive radial and meridional fields).

The near-polar accretion region apparently also extends to low latitudes at phase $\simeq$0.6 in 2008 March, potentially indicating that sporadic non-polar accretion is also occurring at times on TW Hya. This low-latitude appendage directly reflects the $\simeq$30 per cent full-amplitude modulation observed in the emission flux of Ca II (and of He I) profiles peaking around phase 0.6 (see Section 4) and is consistent with veiling estimates (also peaking around phase 0.6 at this epoch). Independent confirmation that this non-polar accretion event is real – rather than caused by overinterpreting intrinsic variability into rotational modulation – comes from the weird Zeeman signatures of Ca II (and He I) lines collected during the emission burst of 2008 March (at cycles 1.654 and 1.668) and excluded from the fitted data set (given their very specific shapes; see Fig. 10). By subtracting the expected Zeeman signatures (the red lines on Fig. 10) from the observed ones (the black lines) for these two profiles, we end up with the Zeeman signatures associated with the excess emission specific to the emission burst and find that they probe a positive radial field, i.e. of polarity opposite to that traced by the main Zeeman signatures collected at similar phases but outside of the accretion burst (e.g. at cycle 3.633). This unambiguously demonstrates that sporadic accretion is truly occurring on TW Hya in regions of positive radial field, i.e. at much lower latitudes than where most of the disc material is accreted (on the pole), therefore validating the reality of the low-latitude appendage to the near-polar accretion region in 2008 March.

6 SUMMARY AND DISCUSSION

We present in this paper new results on magnetospheric accretion processes taking place at the surfaces of forming Sun-like stars; towards this aim, we use spectropolarimetric data collected on the evolved cTTS TW Hya at two different epochs (2008 March and 2010 March) and with ESPaDOnS@CFHT in the framework of the MaPP programme. Strong Zeeman signatures are detected in the LSD profiles of photospheric lines of TW Hya, as well as from the Ca II and He I emission lines commonly used as accretion proxies, revealing the presence of longitudinal fields ranging from −3.5 to 0.7 kG depending on the set of lines and on the observing epoch; in particular, longitudinal fields of opposite polarities are detected (at both epochs) from the two sets of lines (i.e. LSD profiles and accretion proxies), clearly indicating that they probe different regions of the stellar surface. Using our dedicated tomographic imaging tool (tested and validated with several similar studies; e.g. Donati et al. 2010, 2011a, among the most recent ones), we convert these data sets into images of the large-scale magnetic topology, as well as distributions of the photospheric brightness and of the accretion-powered excess emission, at the surface of TW Hya.

We find that the large-scale magnetic field of TW Hya is strong (with a typical average surface intensity of 1.5 kG) and mostly poloidal and axisymmetric (with respect to the rotation axis). More specifically, the poloidal field is dominated by a strong octupole component (with a polar strength of 2.5–2.8 kG) mostly aligned with the rotation axis (to better than 10°) and exhibiting its negative pole to an Earth-based observer. The dipole component is much weaker, by typically a factor of 4–6 (with a polar strength ranging from $\simeq$400 G in 2008 March to $\simeq$700 G in 2010 March), and is found to be mostly antiparallel with respect to the octupole (though apparently tilted at about 45° with respect to the rotation axis in 2008 March). We, however, caution that the latter results need further confirmation from additional data given the fairly strong octupole to dipole intensity contrast and the significant level of intrinsic variability in the data.

Regarding its large-scale magnetic topology, TW Hya is fairly similar to V2129 Oph, also hosting a strong and mostly poloidal, axisymmetric large-scale field in which the octupole component largely dominates (though with parallel, rather than antiparallel, dipole and octupole moments; Donati et al. 2011a); it is, however, significantly different from AA Tau and BP Tau on the one hand (also hosting a strong, mostly axisymmetric, large-scale magnetic field, but with a larger and sometimes dominant dipole component; Donati et al. 2010) and V4046 Sgr, CV Cha or CR Cha on the other hand (exhibiting a much weaker, mostly non-axisymmetric poloidal field; Hussain et al. 2009; Donati et al. 2011b). This is in good agreement with the overall trends on the properties of dynamo fields as derived from previous studies, both on cTTSs and main-sequence dwarfs (e.g. Morin et al. 2008; Donati & Landstreet 2009; Morin et al. 2010); more specifically, these trends show that cool stars (i) are capable of producing intense axisymmetric large-scale fields with strong dipole components when fully convective (as for AA Tau and BP Tau), (ii) start losing their large-scale dipole while keeping a strong axisymmetric octupole when they start developing a radiative core (as for V2129 Oph and TW Hya) and (iii) finally end up with weak, mostly non-axisymmetric poloidal fields when their radiative cores occupy a large-enough proportion of the star (with an outer radius of at least 0.4–0.5 $R_\star$, as for V4046 Sgr, CV Cha and CR Cha).

We also confirm that TW Hya hosts a cool photospheric spot near the pole, as initially proposed by Huélamo et al. (2008) to account for the observed regular RV modulation of its spectrum; we find that this spot is located near the pole, shifted (by about 10°) towards phase 0.35–0.40 (in the ephemeris of equation 1) and apparently very stable on time-scales of several years. This spot mostly overlaps with the main magnetic pole, which thus becomes essentially invisible to LSD photospheric profiles. Most likely, this near-polar, long-lived cool spot is a direct consequence of the strong large-scale magnetic topology, with the intense fields (of $\simeq$3 kG) present at the magnetic pole presumably inhibiting outward energy transport by convection more than everywhere else at the surface of the star. In this respect as well, TW Hya resembles V2129 Oph, which also hosts a similar cool photospheric spot near the pole (Donati et al. 2011a).

We finally obtain that TW Hya hosts a near-polar region of accretion-powered excess Ca II (and He I) emission, mostly overlapping with the cool photospheric spot and coinciding with the main magnetic pole. This confirms in particular that accretion occurs mostly polewards at the surface of TW Hya, again similar to what is reported for V2129 Oph (Donati et al. 2011a). In addition

Downloaded from https://academic.oup.com/mnras/article/417/1/472/980080 by guest on 17 March 2022

to this regular poleward accretion, we also report the detection of sporadic accretion events towards lower latitudes. These episodic events can show up as enhanced rotational modulation in Ca II and He I emission (as in our 2008 March images); they can even manifest themselves at times as short-lived flaring-like emission bursts (as in cycles 1.654 and 1.668) producing specific Zeeman signatures of polarity opposite to (and thus partially cancelling out with) those associated with the main polar accretion region (octupoles exhibiting positive and negative radial fields at low and high latitudes, respectively, or vice versa, within a given hemisphere). We note that the epoch at which equatorward accretion occurs (2008 March) is also that at which the large-scale dipole field is weakest and potentially inclined with respect to the rotation axis (towards the phase of maximum Ca II emission approximately); although this needs confirmation from new data with better phase sampling than our 2008 March data set, it is at least consistent with theoretical expectations (e.g. Romanova et al. 2011).

From the emission fluxes observed in spectral lines commonly used as accretion proxies, we conclude that the logarithmic mass accretion rate at the surface of TW Hya is equal to -8.9 ± 0.4 (in $\mathrm{M_{\odot}\,yr^{-1}}$) at both epochs, in reasonable agreement with recent independent determinations from optical spectra (e.g. Curran et al. 2011). Following the theoretical work of Bessolaz et al. (2008), we can infer that TW Hya is capable of magnetically disrupting its disc up to a distance $r_{\rm mag}$ of about $4 \pm 1\,R_\star$ if the large-scale dipole is as strong as 700 G, but only $3 \pm 1\,R_\star$ if the dipole strength is only 400 G. In the latter case (corresponding to our 2008 March observations), this is just barely beyond the distance at which the dipole field starts to dominate over the octupole field (ranging from 1.7 to $2.2\,R_\star$ for octupole-to-dipole polar strength ratios of 4–6; e.g. Gregory et al. 2010); this potentially explains why equatorward accretion events are observed preferentially at this epoch. When compared to the corotation radius $r_{\rm cor} \simeq 8.3\,R_\star$ (at which the Keplerian period equals the stellar rotation period), we find that $r_{\rm mag}/r_{\rm cor}$ potentially ranges from 0.35 ± 0.10 to 0.50 ± 0.10 depending on the dipole field strength, far below the value (of $\simeq 1$) at which star/disc magnetic coupling can start inducing a significant outflow through a propeller-like mechanism (e.g. Romanova et al. 2004) and thus force the star to spin down and rotate as slowly as one cycle per week.

We thus speculate that TW Hya, with its relatively short rotation period (of $\simeq$3.56 d), is in a phase of rapid spin-up, mostly reflecting the fact that its large-scale dipole field is no longer strong enough to disrupt the disc beyond $0.5\,r_{\rm cor}$ and fuel the associated leak of angular momentum (e.g. through a propeller-like mechanism); this situation is similar, though admittedly not exactly identical, to that described in the recent magnetohydrodynamic simulations of Zanni & Ferreira (2009). In this respect, TW Hya is different from V2129 Oph whose rotation period (of $\simeq$6.53 d) is still rather long. We propose that TW Hya and V2129 Oph are both undergoing a process of rapid spin-up; however, while V2129 Oph is only at the beginning of this phase, TW Hya is in a much more advanced state (suggesting at the same time that TW Hya has been partly convective for a longer time-span than V2129 Oph).

As MaPP observations accumulate and are being analysed, we are progressively building a consistent description of what dynamo magnetic fields of cTTSs look like and how they impact the formation process, in particular regarding the way magnetospheric accretion processes can succeed in slowing down the rotation of cTTSs. More observations are obviously needed to validate more firmly and extend further the initial conclusions drawn from the existing MaPP studies including this one. MaPP is still ongoing, with time granted on ESPaDOnS@CFHT (and with NARVAL, the ESPaDOnS twin mounted on the 2-m Telescope Bernard Lyot at Pic du Midi, in the French Pyrenees) up to semester 2012b; potential extensions, aimed at carrying out a longer survey for a few specific cTTSs and/or at expanding the sample to disc-less T-Tauri stars (also called weak-line T-Tauri stars or wTTSs), are under study at the moment.

ACKNOWLEDGMENTS

We thank the referee for a detailed reading of the manuscript. This paper is based on observations obtained at the Canada–France–Hawaii Telescope (CFHT), operated by the National Research Council of Canada, the Institut National des Sciences de l'Univers of the Centre National de la Recherche Scientifique of France and the University of Hawaii. The 'Magnetic Protostars and Planets' (MaPP) project is supported by the funding agencies of CFHT (through the allocation of telescope time) and by CNRS/INSU in particular, as well as by the French 'Agence Nationale pour la Recherche' (ANR).

REFERENCES

Akeson R. L. et al., 2011, ApJ, 728, 96
Alencar S. H. P., Batalha C., 2002, ApJ, 571, 378
André P., Basu S., Inutsuka S., 2009, The Formation and Evolution of Prestellar Cores. Cambridge Univ. Press, Cambridge, p. 254
Bessell M. S., Castelli F., Plez B., 1998, A&A, 333, 231
Bessolaz N., Zanni C., Ferreira J., Keppens R., Bouvier J., 2008, A&A, 478, 155
Bouvier J., Alencar S. H. P., Harries T. J., Johns-Krull C. M., Romanova M. M., 2007a, in Reipurth B., Jewitt D., Keil K., eds, Protostars and Planets V Magnetospheric Accretion in Classical T Tauri Stars. Univ. Arizona Press, Tucson, p. 479
Bouvier J. et al., 2007b, A&A, 463, 1017
Brickhouse N. S., Cranmer S. R., Dupree A. K., Luna G. J. M., Wolk S., 2010, ApJ, 710, 1835
Calvet N., D'Alessio P., Hartmann L., Wilner D., Walsh A., Sitko M., 2002, ApJ, 568, 1008
Cieza L. A. et al., 2010, ApJ, 712, 925
Curran R. L., Argiroffi C., Sacco G. G., Orlando S., Peres G., Reale F., Maggio A., 2011, A&A, 526, A104
Donati J.-F., 2003, in Trujillo-Bueno J., Sanchez Almeida J., eds, ASP Conf. Ser. Vol. 307, ESPaDOnS: An Echelle SpectroPolarimetric Device for the Observation of Stars at CFHT. Astron. Soc. Pac., San Francisco, p. 41
Donati J., Landstreet J. D., 2009, ARA&A, 47, 333
Donati J.-F., Semel M., Carter B. D., Rees D. E., Collier Cameron A., 1997, MNRAS, 291, 658
Donati J.-F. et al., 2006, MNRAS, 370, 629
Donati J.-F. et al., 2007, MNRAS, 380, 1297
Donati J.-F. et al., 2008a, MNRAS, 385, 1179
Donati J.-F. et al., 2008b, MNRAS, 386, 1234
Donati J. et al., 2010, MNRAS, 409, 1347
Donati J. et al., 2011a, MNRAS, 412, 2454
Donati J. et al., 2011b, MNRAS, in press
Fang M., van Boekel R., Wang W., Carmona A., Sicilia-Aguilar A., Henning T., 2009, A&A, 504, 461
Gregory S. G., Jardine M., Gray C. G., Donati J., 2010, Rep. Progress Phys., 73, 126901
Günther H. M., Schmitt J. H. M. M., Robrade J., Liefke C., 2007, A&A, 466, 1111
Huélamo N. et al., 2008, A&A, 489, L9
Hussain G. A. J. et al., 2009, MNRAS, 398, 189
Johns-Krull C. M., 2007, ApJ, 664, 975

Downloaded from https://academic.oup.com/mnras/article/417/1/472/980080 by guest on 17 March 2022

Kastner J. H., Huenemoerder D. P., Schulz N. S., Canizares C. R., Weintraub D. A., 2002, ApJ, 567, 434
Kurucz R., 1993, CDROM # 13 (ATLAS9 Atmospheric Models) and # 18 (ATLAS9 and SYNTHE Routines, Spectral Line Data Base). Smithsonian Astrophysical Observatory, Washington D. C.
Landi degl'Innocenti E., Landolfi M., 2004, Polarization in Spectral Lines. Kluwer Academic Publishers, Dordrecht
Long M., Romanova M. M., Lovelace R. V. E., 2008, MNRAS, 386, 1274
Morin J. et al., 2008, MNRAS, 390, 567
Morin J., Donati J., Petit P., Delfosse X., Forveille T., Jardine M. M., 2010, MNRAS, 407, 2269
Natta A., Testi L., Muzerolle J., Randich S., Comerón F., Persi P., 2004, A&A, 424, 603
Qi C. et al., 2004, ApJ, 616, L11
Romanova M. M., Ustyugova G. V., Koldoba A. V., Lovelace R. V. E., 2004, ApJ, 616, L151
Romanova M. M., Long M., Lamb F. K., Kulkarni A. K., Donati J., 2011, MNRAS, 411, 915
Rucinski S. M., Krautter J., 1983, A&A, 121, 217
Rucinski S. M. et al., 2008, MNRAS, 391, 1913
Sanchez Almeida J., Lites B. W., 1992, ApJ, 398, 359
Setiawan J., Henning T., Launhardt R., Müller A., Weise P., Kürster M., 2008, Nat, 451, 38
Siess L., Dufour E., Forestini M., 2000, A&A, 358, 593
Thi W. et al., 2010, A&A, 518, L125
Torres G., Guenther E. W., Marschall L. A., Neuhäuser R., Latham D. W., Stefanik R. P., 2003, AJ, 125, 825
Torres C. A. O., Quast G. R., Melo C. H. F., Sterzik M. F., 2008, in Reipurth B., ed., ASP Monograph Publications Vol. 5, Handbook of Star Forming Regions Vol. II. Young Nearby Loose Associations. Astron. Soc. Pac., San Francisco, p. 757
Yang H., Johns-Krull C. M., Valenti J. A., 2005, ApJ, 635, 466
Yang H., Johns-Krull C. M., Valenti J. A., 2007, AJ, 133, 73
Zanni C., Ferreira J., 2009, A&A, 508, 1117

This paper has been typeset from a TEX/LATEX file prepared by the author.

Downloaded from https://academic.oup.com/mnras/article/417/1/472/980080 by guest on 17 March 2022